

The Phoenix Deep Survey: the radio properties of the hard X-ray selected sample

A. Georgakakis^{1*}, A. M. Hopkins^{2†}, J. Afonso³, M. Sullivan^{4,5}, B. Mobasher⁶,
L. E. Cram^{7,8}

¹ *Institute of Astronomy & Astrophysics, National Observatory of Athens, I. Metaxa & B. Pavlou, Penteli, 15236, Athens, Greece*

² *Department of Physics and Astronomy, University of Pittsburgh, 3941 O'Hara Street, Pittsburgh, PA 15260, USA*

³ *Centro de Astronomia e Astrofísica da Universidade de Lisboa, Observatório Astronómico de Lisboa, Lisboa 1349-018, Portugal*

⁴ *Department of Astronomy and Astrophysics, University of Toronto, 60 St. George Street, Toronto, ON M5S 3H8, Canada*

⁵ *Physics Department, University of Durham, Science Labs, South Road, Durham, DH1 3LE*

⁶ *Space Telescope Science Institute, 3700 San Martin Drive, Baltimore, MD 21218, USA*

⁷ *Australian Research Council, GPO Box 9880, Canberra ACT 2601, Australia*

⁸ *The Australian National University, Canberra ACT 0200, Australia*

5 February 2022

ABSTRACT

The radio properties of hard (2–8 keV) X-ray selected sources are explored by combining a single 50 ks XMM-Newton pointing with the ultra-deep and homogeneous Phoenix radio (1.4 GHz) survey (Hopkins et al. 2003). A total of 43 sources are detected above the X-ray flux limit $f_X(2–8 \text{ keV}) = 7.7 \times 10^{-15} \text{ erg s}^{-1} \text{ cm}^{-2}$, with 14 of them exhibiting radio emission above $\approx 40 \mu\text{Jy}$ (3σ). The X-ray/radio matched population lies in the borderline between radio loud and quiet AGNs and comprises sources with both soft and hard X-ray spectral properties suggesting both obscured and unobscured systems. The spectroscopically identified sub-sample (total of 6 X-ray/radio matches) comprises narrow emission line AGNs (4) with hard X-ray spectral properties and broad line sources (2) with soft X-ray spectra. We find evidence that the fraction of X-ray/radio matches increases from $\approx 20\%$ for sources with rest-frame column density $N_{\text{H}} < 10^{22} \text{ cm}^{-2}$ to $\approx 50\%$ for more absorbed systems. Poor statistics however, limit the significance of the above result to the $\approx 2\sigma$ level. Also, the X-ray/radio matched sources have flatter coadded X-ray spectrum ($\Gamma = 1.78_{-0.03}^{+0.05}$) compared to sources without radio emission ($\Gamma = 2.00_{-0.04}^{+0.03}$). A possible explanation for the higher fraction of absorbed sources with radio emission at the μJy level is the presence of circum-nuclear starburst activity that both feeds and obscures the central engine. For a small sub-sample of $z \approx 0.4$ radio emitting AGNs with $N_{\text{H}} > 10^{22} \text{ cm}^{-2}$ their combined spectrum exhibits a soft X-ray component that may be associated with star-formation activity, although other possibilities cannot be excluded. We also find that radio emitting AGNs make up about 13–20 per cent of the hard-band X-ray background depending on the adopted normalisation.

Key words: Surveys – Galaxies: normal – X-rays: galaxies – X-ray: general

1 INTRODUCTION

A key development in X-ray astronomy with the advent of the *Chandra* and the XMM-Newton missions has been the resolution of the bulk of the hard-band X-ray background

(XRB) into discrete sources (e.g. Brandt et al. 2001; Giacomini et al. 2002). Elucidating the nature of these sources however, remains an open issue and has been the subject of intensive observational studies over the last few years. Multiwavelength follow-up programs suggest that the hard X-ray selected population comprises a heterogeneous mix of sources including broad line QSOs and Seyfert 1s, narrow emission-line systems, passive galaxies with absorption line

* email: age@astro.noa.gr

† Hubble Fellow

spectra and optically faint systems with properties suggesting obscured AGN activity at high redshifts (Barger et al. 2002; Mainieri et al. 2002; Fiore et al. 2003; Piconcelli et al. 2003; Georgantopoulos et al. 2004).

Although the above studies have provided a wealth of information on the nature of the sources that make up the bulk of the hard-band XRB there is still limited information on their radio properties. At bright flux limits, $f_X(2 - 10 \text{ keV}) \approx 10^{-13} \text{ erg s}^{-1} \text{ cm}^{-2}$, Akiyama et al. (2000) cross-correlated the ASCA Large Sky Survey with the FIRST radio catalogue, finding an identification rate of ≈ 35 per cent and a fraction of radio-loud hard X-ray selected sources of about 10 per cent. At somewhat fainter fluxes, $f_X(5 - 10 \text{ keV}) \approx 5 \times 10^{-14} \text{ erg s}^{-1} \text{ cm}^{-2}$, Ciliegi et al. (2003) used deeper radio observations to explore the radio properties of the X-ray sources detected in the HELLAS survey. They also find an identification rate of ≈ 30 per cent much higher than that of soft (0.5–2 keV) X-ray selected samples, and argue that this is due to both observational effects (e.g. deeper radio data) and the hard-band selection.

A high fraction (≈ 50 per cent) of hard X-ray selected sources with radio counterparts is also reported by Barger et al. (2001) using deep *Chandra* ($f_X(2 - 10 \text{ keV}) \approx 4 \times 10^{-15} \text{ erg s}^{-1} \text{ cm}^{-2}$) and VLA ($S_{1.4} \approx 25 \mu\text{Jy}$) data. Although these authors do not focus on the radio properties of hard X-ray selected sources, they show that the X-ray/radio matched population contributes as much as 26 per cent of the 2–8 keV XRB. In the 0.5–8 keV spectral band, Bauer et al. (2002) performed a detailed study on the association between faint X-ray and radio sources using the 1 Ms *Chandra* dataset and ultra-deep VLA observations. These authors find that about one third of the X-ray selected AGNs have radio counterparts and argue that the radio emission at least in the sub-sample of harder (i.e. obscured) AGNs is likely to be associated with circum-nuclear star-formation activity. The largest overlap between X-ray and radio sources in the Bauer et al. (2002) study is for the sub-sample of narrow emission line galaxies likely to be star-forming systems. The X-ray sample used by these authors is however, selected in the 0.5–8 keV spectral band and is therefore biased toward soft X-ray sources due to the higher sensitivity of *Chandra* at soft energies.

In this paper we further explore the nature of hard (2–8 keV) X-ray selected sources and their radio properties by combining an ultra-deep and homogeneous radio survey, the Phoenix Deep Survey (PDS; Hopkins et al. 2003), with a single 30 arcmin diameter 50 ksec XMM-*Newton* pointing. These observations are complemented by optical and near-infrared photometry as well as optical spectroscopy. This multiwavelength dataset is referred to here as the Phoenix/XMM-*Newton* survey (Georgakakis et al. 2003). The X-ray data reach a limiting flux of $f_X(2 - 8 \text{ keV}) \approx 7.7 \times 10^{-15} \text{ erg s}^{-1} \text{ cm}^{-2}$, intermediate to brighter X-ray/radio matched samples (e.g. Akiyama et al. 2000; Ciliegi et al. 2003) and deeper surveys (e.g. Barger et al. 2001). The Phoenix/XMM-*Newton* survey also has the advantage of larger areal coverage compared to *Chandra* surveys, due to both the large XMM-*Newton* field-of-view and the wide area and homogeneous radio observations of the PDS. Moreover, in the present study we exploit the unparalleled sensitivity of the XMM-*Newton* (5 times more effective area than

the *Chandra*) to explore the X-ray spectral properties of the detected sources.

Section 2 presents the multiwavelength data (optical, near-infrared, radio and X-ray) available for the PDS, while Section 3 details the sample used in the present study. Our results are presented in Section 4 and discussed in Section 5. Finally, section 6 summarises our conclusions. Throughout this paper we adopt $\Omega_M = 0.3$, $\Omega_\Lambda = 0.7$ and $H_0 = 70 \text{ km s}^{-1} \text{ Mpc}^{-1}$.

2 THE PHOENIX DEEP SURVEY

The Phoenix/XMM-*Newton* survey is a multiwavelength program combining deep radio and X-ray observations with optical and near-infrared data aiming to explore the association between the faint radio and X-ray populations.

2.1 X-ray data

The X-ray data consist of a single 50 ks pointing obtained by the XMM-*Newton* on 2002 May 5 and centered at RA(J2000)=01^h12^m52^s; Dec.(J2000)=−45°33′10.0″. The EPIC (European Photon Imaging Camera; Strüder et al. 2001; Turner et al. 2001) cameras were operated in full frame mode with the medium filter applied.

A full description of the data reduction can be found in Georgakakis et al. (2003). In brief, the Science Analysis Software (SAS 5.3) was used to produce event files for the PN and the two MOS detectors. These were then screened for high particle background periods resulting in PN and MOS good time intervals of 39,444 and 41,273 s respectively. To increase the signal-to-noise ratio and to reach fainter fluxes the PN and the MOS event files have been combined into a single event list using the MERGE task of SAS. Images in celestial coordinates with pixel size of 4.35 arcsec were extracted in the spectral bands 0.5–8 keV (total), 0.5–2 keV (soft) and 2–8 keV (hard) for both the merged and the individual PN and MOS event files. We use the more sensitive (higher S/N ratio) merged image for source detection and flux estimation, while the individual PN and MOS images are used to calculate hardness ratios. This is because the interpretation of hardness ratios is simplified if the extracted count rates are from one detector only.

In this study we use the sources detected in the 2–8 keV band merged image using the EWAVELET task of SAS with a detection threshold of 6σ . These sources were visually inspected and spurious detections clearly associated with CCD gaps, hot pixels or lying close to the edge of the field of view were removed. The final catalogue comprises a total of 43 X-ray sources to the limit $f_X(2 - 8 \text{ keV}) \approx 7.7 \times 10^{-15} \text{ erg s}^{-1} \text{ cm}^{-2}$.

Count rates in the merged (PN+MOS) images as well as the individual PN and MOS images are estimated within an 18 arcsec aperture. For the background estimation we use the background maps generated by the EWAVELET task of SAS. A small fraction of sources lie close to masked regions (CCD gaps or hot pixels) on either the MOS or the PN detectors. This may introduce errors in the estimated source counts. To avoid this bias, the source count rates (and hence the hardness ratios and the flux) are estimated using the

detector (MOS or PN) with no masked pixels in the vicinity of the source.

To convert count rates to flux the Energy Conversion Factors (ECF) of individual detectors are calculated assuming a power law spectrum with $\Gamma = 1.7$ and Galactic absorption $N_{\text{H}} = 2 \times 10^{20} \text{ cm}^{-2}$ appropriate for the Phoenix field (Dickey & Lockman 1990). The mean ECF for the mosaic of all three detectors is estimated by weighting the ECFs of individual detectors by the respective exposure time. For the encircled energy correction, accounting for the energy fraction outside the aperture within which source counts are accumulated, we adopt the calibration given by the XMM-Newton Calibration Documentation [‡].

2.2 Radio data

The radio observations of the Phoenix Deep Survey (PDS[§]) were carried out at the Australia Telescope Compact Array (ATCA) at 1.4 GHz during several campaigns between 1994 and 2001 in the 6A, 6B and 6C array configurations. The data cover a 4.56 square degree area centered at RA(J2000)=01^h11^m13^s Dec.(J2000)=−45°45′00″, much larger than the 30 arcmin diameter region covered by the XMM-Newton observations. A detailed description of the radio observations, data reduction and source detection are discussed by Hopkins et al. (1998, 1999, 2003). The observational strategy adopted resulted in a radio map that is highly homogeneous within the central ≈ 1 deg radius. The 1σ rms noise nevertheless increases from $12\mu\text{Jy}$ at the most sensitive region to about $90\mu\text{Jy}$ close to the field edge. The final catalogue consists of a total of 2148 radio sources to a limit of $60\mu\text{Jy}$ (Hopkins et al. 2003).

The XMM-Newton pointing lies within the most homogeneously covered region of the PDS but is offset from the most sensitive area of the radio map by about 0.30 deg. Therefore, the completeness limit of the radio observations in that 30 arcmin diameter region is $\approx 80\mu\text{Jy}$. The source detection was performed using the False Discovery Rate algorithm described by Hopkins et al. (2002) to robustly quantify the number of spurious sources in radio catalogues. This novel method is somewhat different from the traditional radio source detection algorithms that select sources with peak flux density above a user defined threshold expressed in multiples of the local background RMS noise. Nevertheless, in the region covered by the XMM-Newton the flux density limit of $\approx 80\mu\text{Jy}$ corresponds to a detection threshold for the traditional method of $\approx 5\sigma$. A total of 204 radio sources overlap with the XMM-Newton data.

2.3 Optical and near-infrared photometry

Optical photometric observations of most of the PDS area in the *V* and *R*-bands were obtained at the Anglo-Australian Telescope (AAT) during two observing runs in 1994 and 1995. A detailed description of these observations including data reduction, photometric calibration, source detection and optical identification are presented by Georgakakis

et al. (1999). This dataset is complete to $R = 22.5$ mag. The *U*-band data used in the present study are from the ESO 2.2 m telescope using the WFI on August 18 2001. These observations are described in Sullivan et al. (2004) and reach a completeness limit of $U \approx 22.5$ mag.

Near-infrared observations of the 30 arcmin diameter area covered by the XMM-Newton pointing were obtained using the OSIRIS multi-purpose instrument at the $f/13.5$ focus of the CTIO 1.5-m telescope. The observations were carried out in 2000 December 4-6 in the *J* and *Ks* bands. The OSIRIS is equipped with a 1024×1024 Hawaii HgCdTe array with a field of view of 11×11 arcmin² and a pixel scale of 1.153 arcsec for the $f/2.8$ camera focus position used in our program. To cover the 30 arcmin diameter XMM-Newton pointing we used 7 contiguous pointings.

In the *Ks* band for each pointing a dithering pattern was adopted that consisted of a sequence of 60 s integrations followed by an offset of the telescope. To get accurate sky frames the offset vector was not replicated between successive exposures. The total integration time varied between 20 to 40 min with a mean of 35 min per pointing. In the *J*-band a similar dithering procedure was followed with an exposure time between offsets of 30 to 60 s. The total integration time was 20 min per pointing.

The data reduction was carried out using IRAF tasks. The flat field frame was constructed using both the target observations and the dome flat following a method developed by Peter Witchalls and Will Saunders and described by Sullivan et al. (2004). The sky frame to be subtracted from a given target frame was generated by median combining the 10 images closest in time to the frame in question. All images of the same pointing were registered and coadded to produce the final image. Photometric calibration was carried out using standard stars from Persson et al. (1998). The photometric solutions were stable from night-to-night with a zero-point variation of less than 0.1 mag. The estimated uncertainty in the zero-point is less than 0.02 mag. Astrometric calibration for each field was performed using the positions of at least 20 USNO-2 stars. These solutions were typically accurate to 0.5 arcsec. Source detection used the SEXTRACTOR package (Bertin & Arnouts 1996). Comparing the number counts from these observations with previous studies we estimate a completeness limit of $Ks \approx 18$ mag.

Finally we note that the Phoenix/XMM-Newton field partly overlaps with the deep optical *UBVRI* photometric data presented by Sullivan et al. (2004). These observations use the Wide Field Imager at the AAT (*BVRI* bands) and the CTIO-4m telescopes and reach limiting magnitudes $R \approx 24$ and $U \approx 24$ mag. When available we use these deeper data rather than the shallower observations from either the ESO 2.2m (*U*-band) or our previous AAT survey of the PDS (*VR*-bands). The magnitude given in this study are in the Vega system.

2.4 Optical spectroscopy

A number of X-ray sources in the Phoenix/XMM-Newton field have optical spectroscopic data from the 2dF facility at the AAT as part of the on-going spectroscopic program aiming to obtain spectral information for the optically identified faint radio sources in the PDS. At present redshifts and spectral classifications are available for over 300 radio

[‡] http://xmm.vilspa.esa.es/external/xmm_sw_cal/calib/documentation.shtml#XRT

[§] see also <http://www.atnf.csiro.au/people/ahopkins/phoenix/>

sources brighter than $R = 21.5$ mag. This large dataset is presented by Georgakakis et al. (1999) and Afonso et al. (2004 in preparation).

Additional spectra for both radio and X-ray sources in the Phoenix/XMM-Newton field were obtained with the HYDRA multi-fibre spectrograph at the CTIO Blanco 4-m telescope. A detailed description of these observations as well as the full spectroscopic catalogue will be presented in a future paper (Georgakakis et al. 2004 in preparation). In the present study we concentrate on the HYDRA spectra of the hard X-ray selected sample. In brief, the HYDRA has a 40 arcmin diameter field of view and is equipped with 138 fibres, each 2 arcsec in diameter. The observations were carried out in 2003 August 8-9 in photometric conditions. The grating used was the KPGL2 providing a dispersion of $1.19 \text{ \AA pixel}^{-1}$ and a wavelength resolution of $\approx 8 \text{ \AA}$. To avoid second order contamination we used the GG420 blocking filter. As a result the wavelength coverage of the KPGL2+GG420 combination is $\approx 4200 - 8300 \text{ \AA}$. The total exposure time for each source was 3.5 to 4 h split into 5 or 6 half hour integrations.

The data were reduced using the HYDRA reduction package within IRAF. Fibre flat fields were used to trace the fibre spectra on the CCD and to flat-field the data. Blank sky exposures taken between target observations were employed for throughput calibration. CuArHe arc lamp exposures were employed for wavelength calibration. Redshifts were determined by visual inspection of the resulting spectra. These were then classified into narrow emission line objects, absorption line galaxies and broad emission line systems. Flux calibration has not been performed. This is due to the difficulty in obtaining absolute flux calibration for fibres which can differ substantially in their throughput.

3 THE SAMPLE

The hard (2-8 keV) X-ray selected sample used in the present study comprises a total of 43 sources to the limit $f_X(2 - 8 \text{ keV}) \approx 7.7 \times 10^{-15} \text{ erg s}^{-1} \text{ cm}^{-2}$. These sources were optically identified using the R -band source catalogue by estimating the probability, P , a candidate counterpart is a chance alignment (Downes et al. 1986). Counterpart candidates were searched for within a 6 arcsec radius. We propose 25 secure optical identifications with $P < 0.015$. We also find 5 sources with higher but still acceptable probability being spurious coincidence, $0.015 < P < 0.03$. One source optically identified in the much deeper $BVRI$ optical data presented by Sullivan et al. (2004) lies ≈ 2 arcsec from a very faint $R \approx 24$ mag optical galaxy. Although the probability that this source is a spurious alignment is ≈ 6 per cent we accept the optical identification since the offset between the X-ray and optical positions is within the XMM-Newton positional uncertainty for X-ray bright sources (≈ 3.5 arcsec; McHardy et al. 2003). Summarising, of the 43 hard X-ray selected sources 31 have optical identifications while the remaining 12 are blank fields to the limit $R \approx 22.5$ mag.

The radio and the hard X-ray selected samples were positionally matched using a radius of 6 arcsec. We find a total of 7 sources in common between the two catalogues. We also search for lower significance radio counterparts of hard X-ray selected sources by looking for $> 3\sigma$ peak radio

emission in the vicinity (< 6 arcsec) of X-ray sources. This method further identifies 7 X-ray/radio matches. Given the surface densities of the radio and the X-ray source catalogues the probability of finding by chance a 3σ radio source within 6 arcsec from an X-ray position is estimated to be ≈ 1 per cent.

Redshift measurements are available for 18 hard X-ray selected sources brighter than $R \approx 22$ mag. In addition to these spectroscopic redshifts, for X-ray sources with optical and near-infrared (NIR) photometry in at least 4 bands and relatively hard X-ray spectral properties, $\text{HR} > -0.4$ (corresponding to observed column densities in excess of 10^{21} cm^{-2} ; $\Gamma = 1.7$) we also estimate photometric redshifts using galaxy templates and methods outlined in Sullivan et al. (2004). These sources have colours suggesting that their optical emission is dominated by light from the host galaxy rather than the central AGN, thus allowing templates for normal galaxies to be used (see section 4; Barger et al. 2002, 2003; Mobasher et al. 2004; Gandhi et al. 2004). Comparing z_{phot} with z_{spec} for the 5 sources with (i) $\text{HR} > -0.4$, (ii) at least 4-band photometry and (iii) available spectroscopy we estimate the accuracy of our method to be $|\delta z|/z_{\text{spec}} \approx 0.1$. Although the statistics are poor the above result indicates that templates for normal galaxies can successfully be used to estimate photometric redshifts for the X-ray harder sources (see also Barger et al. 2002, 2003; Mobasher et al. 2004; Gandhi et al. 2004). This method provides photometric redshift estimates for 3 sources that have no spectroscopic redshift measurement. X-ray sources with soft X-ray spectral properties are most likely dominated by light from the central AGN (see section 4), although we caution the reader that there is increasing evidence for broad line AGNs that do not behave this way and show flat (hard) X-ray spectra (Risaliti et al. 2001; Risaliti et al. 2003). Unlike galaxies, estimating photometric redshifts for AGN dominated systems is challenging and despite recent progress the results are significantly less accurate (Richards et al. 2001; Kitsionas et al. 2004; Babbedge et al. 2004). In the present study we do not estimate photometric redshifts for sources with soft X-ray spectral properties likely to be Seyfert 1s or QSOs.

One of the hard X-ray selected sources (#25 in Table 1 below) has a very bright, $R \approx 13$ mag, optically unresolved counterpart and very low X-ray-to-optical flux ratio ($\log f_X/f_{\text{opt}} \approx -3$). Also, as discussed in Appendix A the X-ray spectrum of this object is best fit by a Raymond-Smith hot gas model (Raymond & Smith 1977) with temperature $kT = 0.7$ keV. Although optical spectroscopy is not available the evidence above indicates that this X-ray source is associated with a Galactic star. In the rest of this paper we will not consider this source in our analysis.

The hard X-ray selected sample used in this paper is presented in Table 1 which has the following format:

1. Identification number.
- 2-3. Right ascension and declination of the X-ray centroid position in J2000.
- 4-7 U , V , R and K -band magnitudes (Vega based system) respectively of the optical counterpart if available.
8. Probability, P , the optical counterpart is a chance coincidence.
9. Offset in arcseconds between the X-ray and optical source positions.

10. Spectroscopic or photometric redshift.

11. Quality, Q , of the redshift estimate. A value $Q = 3$ corresponds to three or more identified spectral features indicating a reliable redshift. A value $Q = 1, 2$ corresponds to 1 and 2 identified spectral features respectively.

12. Classification on the basis of the observed optical spectral features: **AB**: absorption lines only; **NL**: narrow emission lines; **BL**: broad emission lines.

13. Radio flux density, $S_{1.4}$, of the radio counterpart of the X-ray source if available. Radio sources that lie below the formal limit $S_{1.4} \approx 80 \mu\text{Jy}$ of the radio catalogue corresponding to about 5σ are marked. Although the peak flux density of these sources is below the 5σ level their integrated flux density is, in some cases, brighter than $80 \mu\text{Jy}$.

14. Offset in arcseconds between the radio and X-ray source positions.

We further explore the X-ray spectral properties of the present sample using the XSPEC v11.2 package. For sources with small number of net counts we use the C-statistic technique (Cash 1979) specifically developed to extract information from low signal-to-noise ratio spectra. The data are grouped to have at least one count per bin. We note however, that higher binning factors or no binning does not change our results. Firstly, we attempt to constrain the N_{H} by fitting an absorbed (Wisconsin cross-sections; Morrison and McCammon 1983) power-law model (wabs*pow) fixing the power-law index to $\Gamma = 1.7$. This value of Γ is selected to be inbetween the mean spectral index of radio loud ($\Gamma = 1.6$; Reeves & Turner 2000; Gambill 2003) and radio quiet AGNs ($\Gamma \approx 1.9$; Laor et al. 1997; Reeves & Turner 2000). We then use the same model (wabs*pow) to estimate the power law index Γ keeping the column density fixed to the Galactic value ($N_{\text{H}} = 2 \times 10^{20} \text{ cm}^{-2}$). For sources with sufficient counts we perform standard χ^2 spectral fitting. The data were grouped to have a minimum of 15 counts per bin to ensure that Gaussian statistics apply. For the χ^2 analysis we require that the source spectrum has at least 15 spectral bins. An absorbed power-law (wabs*pow) is fit to the data yielding the intrinsic absorbing column density (i.e. after subtracting the Galactic absorption) and the power-law photon index Γ . This model provides acceptable fits (i.e. reduced $\chi^2 \approx 1$) for all sources. The parameters estimated from the C-statistic and the χ^2 analysis are consistent within the errors. For both the χ^2 and the C-statistic analysis the fit was performed in the 0.2-8 keV energy range where the sensitivity of the XMM-Newton is the highest. The estimated errors correspond to the 90 per cent confidence level. The results of the above X-ray spectral analysis along with the X-ray properties of the sample are presented in Table 2 which has the following format:

1. Identification number.
2. 2-8 keV X-ray flux in $\text{erg s}^{-1} \text{ cm}^{-2}$.
3. Hardness ratio, HR, defined as

$$\text{HR} = \frac{\text{RATE}(2080) - \text{RATE}(0520)}{\text{RATE}(2080) + \text{RATE}(0520)}, \quad (1)$$

where RATE(0520) and RATE(2080) are the count rates in the 0.5-2 and 2-8 keV spectral bands respectively. For sources with less than 5 net counts in either the hard or the soft bands a lower or an upper limit (3σ) respectively is estimated for the hardness ratio assuming Poisson statistics. The hardness ratios are estimated using the PN data

except for sources that lie close to PN CCD gaps or hot pixels where we use MOS data (see section 2.1). These sources are marked in Table 2.

4. Column density N_{H} estimated by either the C-statistic method assuming $\Gamma = 1.7$ or the standard χ^2 spectral fitting in the case of sources with sufficient counts (see discussion above).

5. Power law spectral index Γ estimated by either the C-statistic for a fixed Galactic column density $N_{\text{H}} = 2 \times 10^{20} \text{ cm}^{-2}$ or the standard χ^2 spectral fitting in the case of sources with sufficient counts (see discussion above).

6. 2-8 keV X-ray luminosity if a spectroscopic or photometric redshift is available. For the k-correction we assume $\Gamma = 1.7$.

7. 1.4 GHz radio power if a spectroscopic or photometric redshift is available, adopting a radio spectral index $\alpha = 0.8$ for the k-correction.

Summarising the information presented in Tables 1 and 2 the hard X-ray selected sample comprises: (i) 11 AGNs with broad emission lines, (ii) 6 systems with narrow emission line optical spectra, (iii) 1 galaxy with absorption optical lines, (iv) 1 Galactic star candidate on the basis of its optical and X-ray properties, (v) 3 sources with photometric redshift estimates, (vi) 9 sources with optical identification but no redshift information most of which have soft X-ray spectral properties suggesting AGNs and (vii) 12 optically unidentified sources. For the X-ray/radio matched population 4 sources are associated with narrow emission line systems, 2 show broad emission lines and 8 sources with no spectroscopic identification. Notes on individual optically identified X-ray sources with radio counterparts and available spectroscopic information are presented in Appendix A. This appendix includes the optical and X-ray spectra as well as the optical images, with the X-ray contours overlaid, of individual radio sources (Figures A1, A2 and A3). Also most of the sources with radio counterparts in the present study lie in the border line between radio-loud and quiet systems ($\alpha_{\text{RO}} \approx 0.35$; Stocke et al. 1991; Ciliegi et al. 2003).

We note that source #12 in Tables 1 and 2 is assigned a redshift $z = 0.985$ on the basis of a single narrow emission line interpreted as [O II] 3727 Å. The X-ray spectrum suggests heavy obscuration corresponding to a rest-frame column density (i.e. after correcting for redshift) of $N_{\text{H}} \approx 10^{23} \text{ cm}^{-2}$ ($\Gamma = 1.7$). The X-ray luminosity of this source at $z = 0.985$ before applying any correction due to intrinsic photoelectric absorption is estimated $L_X(2 - 8 \text{ keV}) \approx 10^{44} \text{ erg s}^{-1} \text{ cm}^2$. The evidence above suggests a candidate type-2 QSO, although more observations are required to confirm the redshift measurements and to search for broad emission line components. More details on the properties of this source are given in Appendix A.

4 RESULTS

4.1 X-ray and optical properties of the sample

Figure 1 plots R -band magnitude against 2-8 keV X-ray flux. The $\log(f_X/f_{\text{opt}}) = \pm 1$ lines in this figure delineate the region of the parameter space occupied by powerful unobscured AGNs (Stocke et al. 1991). The X-ray-to-optical flux ratio is estimated from the relation

ID	α_X (J2000)	δ_X (J2000)	U (mag)	V (mag)	R (mag)	K (mag)	P ($\times 10^{-3}$)	δ_{XO} ('')	z	Q	class ^a	$S_{1.4}$ (mJy)	δ_{XR} ('')
1	14 05.4	-45 32 19	21.06 ± 0.06	—	20.15 ± 0.03	17.56 ± 0.12	2.2	1.3	1.160	2	BL	—	—
2	14 00.4	-45 34 42	21.33 ± 0.07	—	20.30 ± 0.04	17.50 ± 0.12	0.2	0.4	0.406	2	NL	—	—
3	13 58.5	-45 39 11	19.69 ± 0.02	—	20.65 ± 0.05	> 18	17.1	3.0	1.385	3	BL	—	—
4	13 49.8	-45 27 02	21.83 ± 0.09	—	20.49 ± 0.04	18.08 ± 0.18	< 0.1	0.1	—	—	—	—	—
5	13 39.8	-45 32 31	21.13 ± 0.05	20.73 ± 0.03	—	18.41 ± 0.29	0.5	0.6	2.329	3	BL	—	—
6	13 37.6	-45 31 45	> 22.5	22.55 ± 0.13	—	> 18	20.5	2.3	—	—	—	—	—
7	13 33.2	-45 38 42	20.52 ± 0.06	19.52 ± 0.02	18.49 ± 0.01	15.72 ± 0.06	0.4	0.9	0.276	3	NL	0.472	1.4
8	13 31.9	-45 36 28	22.89 ± 0.23	22.04 ± 0.12	21.1 ± 0.05	17.90 ± 0.16	26.5	3.2	0.516	1	NL	—	—
9	13 31.7	-45 44 43	> 22.5	> 23	> 22.5	> 18	—	—	—	—	—	—	—
10	13 27.0	-45 38 32	19.73 ± 0.02	19.99 ± 0.02	19.62 ± 0.01	17.84 ± 0.28	4.5	2.2	1.220	2	BL	—	—
11	13 19.9	-45 32 58	> 22.5	> 23	> 22.5	> 18	—	—	—	—	—	—	—
12	13 14.6	-45 40 52	22.32 ± 0.19	22.09 ± 0.14	22.03 ± 0.15	> 18	4.9	1.1	0.985	1	NL	1.027	1.8
13	13 11.5	-45 24 01	20.48 ± 0.03	20.12 ± 0.02	19.46 ± 0.01	16.68 ± 0.07	0.5	0.8	0.299	3	BL	0.125 ^e	4.7
14	13 10.7	-45 38 20	21.90 ± 0.10	21.41 ± 0.06	21.34 ± 0.06	> 18	9.5	1.9	—	—	—	0.039 ^e	3.5
15	13 09.9	-45 41 37	> 22.5	> 23	> 22.5	> 18	—	—	—	—	—	—	—
16	13 09.9	-45 32 30	> 22.5	> 23	> 22.5	> 18	—	—	—	—	—	—	—
17	13 06.3	-45 45 18	19.98 ± 0.04	18.45 ± 0.01	17.67 ± 0.03	14.58 ± 0.03	6.1	4.7	0.235	3	AB	—	—
18	13 02.8	-45 24 41	> 22.5	22.55 ± 0.13	—	> 18	18.0	1.3	—	—	—	—	—
19	13 02.0	-45 30 22	18.85 ± 0.01	19.54 ± 0.01	19.22 ± 0.01	17.83 ± 0.15	0.2	0.7	1.208	1	BL	—	—
20	13 01.1	-45 38 47	> 22.5	> 23	> 22.5	18.65 ± 0.38	—	—	—	—	—	0.063 ^e	1.2
21	13 00.0	-45 37 17	> 22.5	—	22.34 ± 0.16	18.00 ± 0.25	4.2	0.6	—	—	—	—	—
22	12 59.1	-45 23 43	> 22.5	20.98 ± 0.06	20.00 ± 0.02	17.08 ± 0.09	1.5	1.0	0.369	3	NL	0.078 ^e	2.4
23 ^b	12 58.8	-45 38 22	18.98 ± 0.01	19.89 ± 0.01	19.75 ± 0.02	17.87 ± 0.13	2.2	1.5	1.975	3	BL	0.420 ^e	4.9
24	12 57.0	-45 29 43	22.38 ± 0.17	22.19 ± 0.15	21.78 ± 0.09	> 18	10.9	1.7	1.550	1	BL	—	—
25 ^c	12 51.7	-45 23 54	15.57 ± 0.01	13.88 ± 0.01	13.07 ± 0.01	11.01 ± 0.02	0.1	2.0	—	—	STAR?	—	—
26	12 49.9	-45 32 55	> 22.5	> 23	> 22.5	> 18	—	—	—	—	—	—	—
27	12 46.2	-45 40 15	> 22.5	> 23	> 22.5	> 18	—	—	—	—	—	—	—
28	12 43.8	-45 42 50	22.29 ± 0.07	22.75 ± 0.13	21.60 ± 0.01	17.69 ± 0.16	1.7	2.1	0.776	—	photo-z	0.062 ^e	2.3
29 ^b	12 43.7	-45 35 45	23.72 ± 0.15	23.84 ± 0.19	23.41 ± 0.03	> 18	23.0	1.5	—	—	—	0.077	0.1
30	12 42.2	-45 28 39	20.58 ± 0.03	21.15 ± 0.06	20.85 ± 0.04	18.79 ± 0.45	4.4	1.5	—	—	—	—	—
31	12 40.5	-45 38 41	> 22.5	> 23	> 22.5	> 18	—	—	—	—	—	0.137	0.5
32	12 32.3	-45 35 20	20.51 ± 0.03	20.58 ± 0.04	19.95 ± 0.02	> 18	2.0	1.2	—	—	—	0.070 ^e	0.3
33	12 28.0	-45 26 41	> 22.5	22.55 ± 0.13	—	> 18	—	—	—	—	—	0.121	2.1
34 ^b	12 27.1	-45 44 27	20.64 ± 0.01	21.30 ± 0.01	21.09 ± 0.01	18.43 ± 0.40	6.5	1.9	1.010	2	BL	—	—
35	12 23.1	-45 24 56	> 22.5	> 23	> 22.5	—	—	—	—	—	—	—	—
36 ^b	12 15.0	-45 31 00	23.15 ± 0.01	22.39 ± 0.04	21.34 ± 0.01	17.7 ± 0.13	3.9	1.0	0.842	—	photo-z	—	—
37 ^b	12 13.8	-45 45 52	19.39 ± 0.01	19.80 ± 0.01	19.67 ± 0.01	—	2.5	1.6	0.922	3	BL	—	—
38	12 12.5	-45 27 47	> 22.5	> 23	> 22.5	—	—	—	—	—	—	0.181	2.8
39	12 10.1	-45 30 05	> 22.5	> 23	> 22.5	> 18	—	—	—	—	—	—	—
40 ^{bd}	12 04.8	-45 35 32	> 25	24.80 ± 0.30	23.85 ± 0.10	> 18	62.5	2.0	0.732	—	photo-z	—	—
41	12 04.6	-45 25 49	21.16 ± 0.03	21.55 ± 0.06	21.27 ± 0.04	—	3.8	1.2	1.200	1	BL	—	—
42 ^b	11 50.2	-45 37 25	21.25 ± 0.03	20.37 ± 0.01	19.46 ± 0.01	—	2.8	2.1	0.493	3	NL	0.135	2.1
43 ^b	11 41.9	-45 40 01	20.99 ± 0.01	20.46 ± 0.01	19.78 ± 0.01	—	3.0	1.8	—	—	—	—	—

^a AB: absorption lines; NL: Narrow emission lines; BL: Broad emission lines; photo-z: photometric redshift

^b UV and optical data are from Sullivan et al. (2004)

^c Optical and X-ray properties indicating Galactic star

^d source #40: although $P > 0.05$ the optical ID is included in the sample since δ_{OX} is within the XMM-Newton positional uncertainty.

^e lower significance radio source with peak flux density in the range $3 - 5\sigma$. Not included in the Hopkins et al. (2003) radio catalogue.

Table 1. Phoenix/XMM-Newton survey: optical and radio properties of the hard X-ray selected sample.

$$\log \frac{f_X}{f_{opt}} = \log f_X(2 - 8 \text{ keV}) + 0.4 R + 5.53. \quad (2)$$

The equation above is derived from the X-ray-to-optical flux ratio definition of Stocke et al. (1991) that involved 0.3-3.5 keV flux and V -band magnitude. These quantities are converted to 2-8 keV flux and R -band magnitude assuming a mean colour $V - R = 0.7$ and a power-law X-ray spectral energy distribution with index $\Gamma = 1.7$. In Figure 1 all the extragalactic hard X-ray selected sources lie in the AGN region of the parameter space (i.e. between the $\log f_X/f_{opt} \pm 1$ diagonal lines). Hard X-ray sources with radio counterparts have a range of X-ray-to-optical flux ratios.

Optical unidentified sources are shown as upper limits in this figure. Some of them lie above the upper bound of the empirical AGN envelope defined by Stocke et al. (1991) suggesting high redshift and/or dust obscuration (Alexander et al. 2001; Brusa et al. 2003; Fiore et al. 2003; Gandhi et al. 2004; Mignoli et al. 2004; Georgantopoulos et al. 2004). Although none of these sources is detected in

our relatively shallow K -band survey ($K = 18$ mag) they have, on average, hard X-ray spectral properties. This is shown in Figure 2 plotting hardness ratio (equation 1) as a function of the X-ray-to-optical flux ratio (equation 2). Optically unidentified sources with $\log f_X/f_{opt} \gtrsim +1$ have $HR > -0.2$ suggesting enhanced observed photoelectric absorption ($N_H > 3 \times 10^{21} \text{ cm}^{-2}$, $\Gamma = 1.7$). Also, in Figure 2 there is fair agreement between the X-ray and optical spectroscopic properties of our sources. Spectroscopically confirmed broad-line AGNs have soft X-ray spectra, while narrow emission-line systems have, on average, HRs suggesting observed absorbing columns in excess of 10^{21} cm^{-2} ($\Gamma = 1.7$).

We further compare the X-ray and optical/NIR properties of the present sample in Figure 3 plotting the hardness ratio against $R - K$ colours. Although, there is large scatter in this Figure, the obscured (high HR) X-ray sources are, on average, redder than those with softer X-ray spectral properties. This suggests that the optical/NIR light of X-ray

ID	$f_X(2-8\text{ keV})$ ($\times 10^{-14}\text{ erg s}^{-1}\text{ cm}^{-2}$)	HR	N_{H}^a (10^{21} cm^{-2})	Γ	$\log L_X(2-8\text{ keV})$ (erg s^{-1})	$\log L_{1.4}$ (W Hz^{-1})
1	3.39 ± 0.46	-0.51 ± 0.09	< 0.52	$1.99^{+0.35}_{-0.26}$	44.40 ± 3.41	—
2 ^b	1.47 ± 0.48	-0.70 ± 0.10	< 0.19	$2.69^{+0.27}_{-0.27}$	42.97 ± 1.36	—
3	2.87 ± 0.47	-0.36 ± 0.11	< 0.19	$2.02^{+0.27}_{-0.23}$	44.51 ± 2.86	—
4 ^{bc}	0.89 ± 0.41	-0.59 ± 0.17	< 0.09	$2.42^{+0.26}_{-0.32}$	—	—
5	1.60 ± 0.30	-0.66 ± 0.09	< 0.56	$1.94^{+0.42}_{-0.21}$	44.78 ± 2.55	—
6 ^c	1.23 ± 0.28	-0.28 ± 0.18	$2.70^{+2.28}_{-1.00}$	$1.23^{+0.22}_{-0.24}$	—	—
7 ^c	6.66 ± 0.51	$+0.49 \pm 0.09$	$21.79^{+0.91}_{-4.39}$	$0.33^{+0.12}_{-0.24}$	43.25 ± 5.76	23.21
8 ^{bc}	1.07 ± 0.36	-0.14 ± 0.22	$7.06^{+10.84}_{-1.76}$	$0.84^{+0.18}_{-0.43}$	43.08 ± 1.32	—
9 ^c	3.08 ± 0.50	-0.03 ± 0.17	$13.30^{+9.30}_{-4.80}$	$0.89^{+0.36}_{-0.49}$	—	—
10	2.34 ± 0.43	-0.61 ± 0.07	$0.20^{+0.39}_{-0.20}$	$2.35^{+0.31}_{-0.25}$	44.29 ± 2.55	—
11	1.29 ± 0.23	-0.50 ± 0.13	< 1.40	$1.67^{+0.60}_{-0.27}$	—	—
12 ^c	2.10 ± 0.35	$+0.51 \pm 0.24$	$22.4^{+13.30}_{-7.90}$	$0.36^{+0.35}_{-0.36}$	44.03 ± 2.75	25.01
13	1.28 ± 0.31	-0.71 ± 0.09	< 0.5	$2.54^{+0.37}_{-0.17}$	42.61 ± 1.82	22.71
14	1.62 ± 0.27	-0.55 ± 0.11	$0.11^{+0.70}_{-0.11}$	$1.74^{+0.35}_{-0.24}$	—	—
15 ^c	1.55 ± 0.34	$+0.30 \pm 0.30$	$10.20^{+7.20}_{-3.60}$	$0.43^{+0.41}_{-0.36}$	—	—
16 ^b	1.21 ± 0.28	-0.43 ± 0.11	< 1.40	$2.02^{+0.58}_{-0.28}$	—	—
17	2.96 ± 0.51	-0.41 ± 0.12	< 0.97	$1.58^{+0.54}_{-0.27}$	42.73 ± 2.57	—
18	2.00 ± 0.32	-0.56 ± 0.10	$0.70^{+0.90}_{-0.70}$	$2.00^{+0.49}_{-0.22}$	—	—
19	1.59 ± 0.22	-0.86 ± 0.05	< 0.04	$3.27^{+0.07}_{-0.14}$	44.12 ± 3.32	—
20 ^c	0.95 ± 0.25	$+0.32 \pm 0.43$	$51.67^{+39.53}_{-23.47}$	$-0.25^{+0.66}_{-0.87}$	—	—
21 ^b	1.13 ± 0.31	-0.65 ± 0.10	$0.84^{+0.96}_{-0.84}$	$2.24^{+0.53}_{-0.49}$	—	—
22 ^c	1.28 ± 0.31	> 0.13	$68.4^{+59.60}_{-30.90}$	$-0.63^{+0.91}_{-0.88}$	42.81 ± 1.83	22.73
23	0.94 ± 0.23	-0.48 ± 0.16	< 0.16	$1.58^{+0.65}_{-0.43}$	44.39 ± 1.95	25.51
24	0.79 ± 0.19	-0.46 ± 0.13	< 0.28	$2.20^{+0.34}_{-0.32}$	44.07 ± 1.97	—
25 ^d	1.73 ± 0.34	-0.91 ± 0.04	—	—	—	—
26 ^c	0.27 ± 0.15	-0.38 ± 0.44	$0.55^{+0.75}_{-0.55}$	$1.62^{+0.40}_{-0.38}$	—	—
27	1.44 ± 0.30	-0.51 ± 0.12	$0.29^{+1.41}_{-0.29}$	$1.89^{+0.58}_{-0.30}$	—	—
28 ^c	1.00 ± 0.40	$+0.22 \pm 0.33$	$8.20^{+5.20}_{-3.60}$	$0.91^{+0.33}_{-0.37}$	43.46 ± 1.14	23.50
29 ^{bc}	0.91 ± 0.27	$+0.08 \pm 0.25$	< 0.10	$2.09^{+0.32}_{-0.33}$	—	—
30	1.22 ± 0.22	-0.54 ± 0.10	< 0.33	$2.11^{+0.26}_{-0.22}$	—	—
31	2.35 ± 0.36	-0.18 ± 0.10	$1.20^{+3.50}_{-1.20}$	$1.59^{+0.57}_{-0.32}$	—	—
32	12.4 ± 0.51	-0.60 ± 0.02	< 0.03	$2.10^{+0.05}_{-0.04}$	—	—
33 ^c	1.70 ± 0.29	-0.26 ± 0.16	$4.30^{+1.50}_{-2.50}$	$1.02^{+0.10}_{-0.20}$	—	—
34	3.37 ± 0.57	-0.62 ± 0.09	$0.27^{+0.84}_{-0.27}$	$2.00^{+0.30}_{-0.40}$	44.26 ± 2.71	—
35 ^{bc}	3.20 ± 0.53	$+0.41 \pm 0.15$	$14.28^{+6.51}_{-3.29}$	$0.39^{+0.26}_{-0.26}$	—	—
36 ^c	0.80 ± 0.23	$+0.19 \pm 0.53$	$9.90^{+12.20}_{-4.50}$	$0.75^{+0.42}_{-0.44}$	43.45 ± 1.54	—
37	4.95 ± 0.83	-0.46 ± 0.08	< 0.29	$1.96^{+0.21}_{-0.17}$	44.33 ± 2.73	—
38 ^c	0.94 ± 0.28	-0.13 ± 0.24	$2.34^{+3.36}_{-2.27}$	$1.38^{+0.50}_{-0.50}$	—	—
39 ^c	0.76 ± 0.26	$+0.13 \pm 0.56$	$5.50^{+7.70}_{-3.50}$	$0.99^{+0.49}_{-0.55}$	—	—
40 ^c	1.19 ± 0.3	-0.36 ± 0.26	$4.3^{+3.6}_{-1.9}$	$0.98^{+0.27}_{-0.28}$	43.48 ± 1.78	—
41	1.85 ± 0.37	-0.59 ± 0.11	< 0.78	$2.00^{+0.49}_{-0.22}$	44.18 ± 2.31	—
42 ^c	1.45 ± 0.40	> -0.24	$68.7^{+68.6}_{-37.2}$	$-0.27^{+0.68}_{-0.71}$	43.16 ± 1.6	23.3
43	5.81 ± 0.67	-0.48 ± 0.08	$0.19^{+0.59}_{-0.19}$	$2.04^{+0.35}_{-0.27}$	—	—

^aObserved column density not corrected for redshift

^bflux and hardness ratio from the MOS detector

^c N_{H} and Γ estimated using the C-statistic method.

^dGalactic star candidate. Best fit by a Raymond-Smith model, $kT=0.7$, abundance=0.04

Table 2. Phoenix/XMM-Newton survey: The X-ray properties, X-ray and radio luminosities of the sample

harder sources is dominated by the host galaxy rather than the obscured central AGN (Barger et al. 2002, 2003; Brusa et al. 2003; Fiore et al. 2003; Mignoli et al. 2004; Gandhi et al. 2004; Georgantopoulos et al. 2004). This is demonstrated in Figure 4 where we plot $R - K$ and $V - R$ colours as a function of redshift. Overlaid are the optical/NIR colours of a QSO spectrum (Cristiani & Vio 1990; Cristiani et al. 2004; obtained from the template SEDs of the LE PHARE

software[¶]) and the mean observed spectra of four different galaxy types (E/S0, Sbc, Scd, Im) from Coleman, Wu & Weedman (1980). Broad line AGNs, most of which exhibit soft X-ray spectra, have colours consistent with the QSO template prediction, while the X-ray harder sources follow

[¶] http://www.lam.oamp.fr/arnouts/LE_PHARE.html

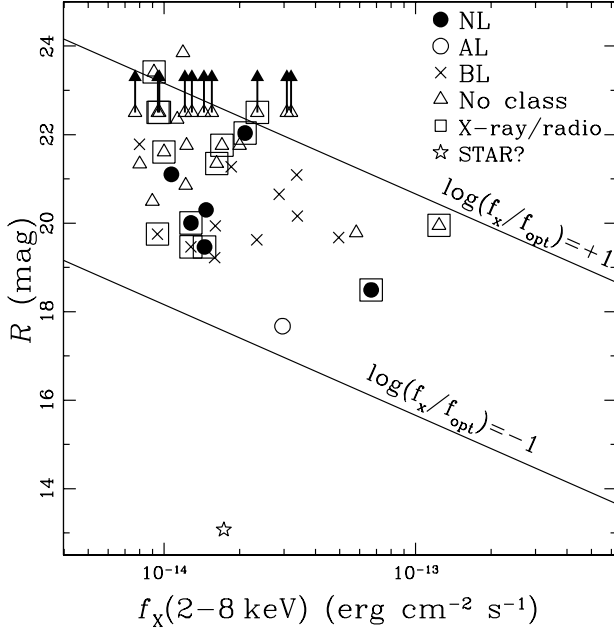


Figure 1. R -band magnitude against 2-8 keV flux. Filled circles are for sources with narrow emission line optical spectra, open circles correspond to absorption line systems, while crosses signify broad optical emission lines. Sources with no spectroscopic classification are shown with a triangle. A square on top of a symbol is for X-ray/radio matched sources. Optically unidentified objects as plotted as upper limits. The star is for the Galactic star candidate in the present sample. The lines indicate constant X-ray-to-optical flux ratios of $+1$ and -1 . The lines $\log f_X/f_{opt} = \pm 1$ delineate the region of the parameter space occupied by powerful unobscured AGNs.

the galaxy tracks in Figure 4. The evidence above justifies the use of galaxy SEDs to estimate photometric redshifts for the X-ray harder sources in section 3.

In Figures 2, 3 there is evidence for a higher fraction of X-ray/radio matches within the harder (i.e. higher hardness ratio) X-ray population. This is further explored in Figure 5, where we plot the distribution of the HR and the *rest-frame* column density (i.e. after correcting for the redshift) of both the hard X-ray selected sample and the X-ray/radio matched population. The N_H at the *observer's frame* is estimated from the χ^2 X-ray spectral fittings described in section 3. In the case of X-ray spectra with small number of counts we adopt the N_H values estimated by the C-statistic method assuming a spectral index $\Gamma = 1.7$. The *observer's frame* column density however, is lower than the *rest-frame* one because the k -effect shifts the absorption turnover to lower energies. The relation between the intrinsic rest-frame and the observed column density scales approximately as $(1+z)^{2.65}$ (e.g. Barger et al. 2002). This correction is applied to all the sources in the sample before plotting the histogram in Figure 5. For sources without spectroscopic identification we assume a mean redshift $z = 1$, similar to the peak of the redshift distribution of the hard X-ray population (e.g. Fiore et al. 2003). Also, sources with X-ray spectra consistent with no absorption above the Galactic are plotted at the Galactic column density, $N_H = 2 \times 10^{20} \text{ cm}^{-2}$.

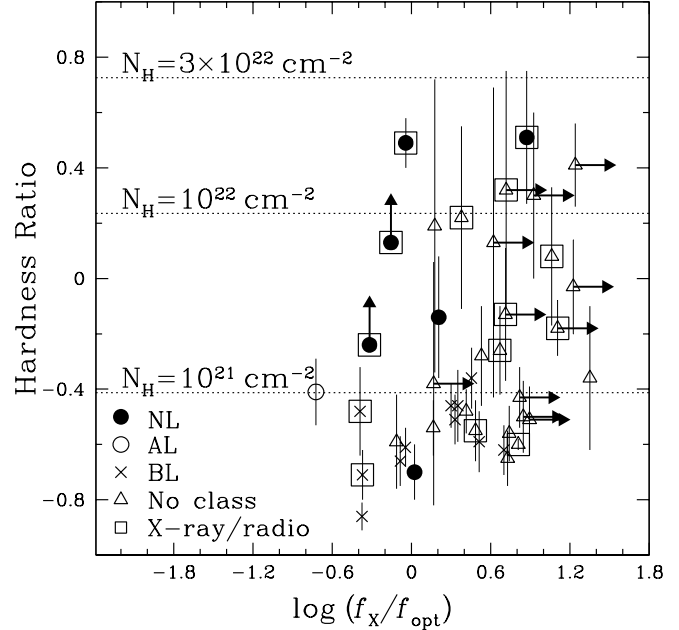


Figure 2. Hardness ratio against X-ray-to-optical flux ratio as defined in section equation 2. The symbols are the same as in Figure 1. Sources that have less than 5 net counts in either the hard or the soft spectral bands are plotted as lower or upper limits respectively. The horizontal lines are the expected hardness ratio of a power-law spectral energy distribution with $\Gamma = 1.7$ and different absorbing column densities in the range 0.1 to $3 \times 10^{22} \text{ cm}^{-2}$.

Figure 5 suggests that the fraction of X-ray/radio matches increases with the HR or the N_H . About 18 per cent (4/22) of the population with $HR < -0.4$ is associated with radio emission while 50 per cent (10/20) of the $HR > -0.4$ sources have radio counterparts. Similarly, the fraction of X-ray/radio matches is about 23 per cent (6/26) of the population with rest-frame column density $N_H < 10^{22} \text{ cm}^{-2}$ and increases to about 50 per cent (8/16) for $N_H > 10^{22} \text{ cm}^{-2}$. However, the small sample size may bias our conclusions. We therefore compare the HR and N_H distributions of X-ray selected AGNs with and without radio counterparts using the Gehan's statistical test as implemented in the ASURV package (Isobe, Feigelson & Nelson 1986; LaValley, Isobe & Feigelson 1992). The probability the two distributions are drawn from the same parent population is rejected at the ≈ 95 per cent confidence level corresponding to about 2σ .

4.2 X-ray spectra

In this section we focus on the X-ray spectra of both individual sources and different groups of X-ray selected AGNs. Firstly, we compare the X-ray spectral properties of the AGNs with and without radio counterparts, comprising 14 and 28 systems respectively. The individual spectra of sources in these sub-samples are merged using the MATHPHA task of FTOOLS to produce 3 independent coadded spectral files for the PN, MOS1 and MOS2 detectors respectively. The combined spectra are grouped to a minimum of 15 counts per bin to ensure that Gaussian statistics apply. The

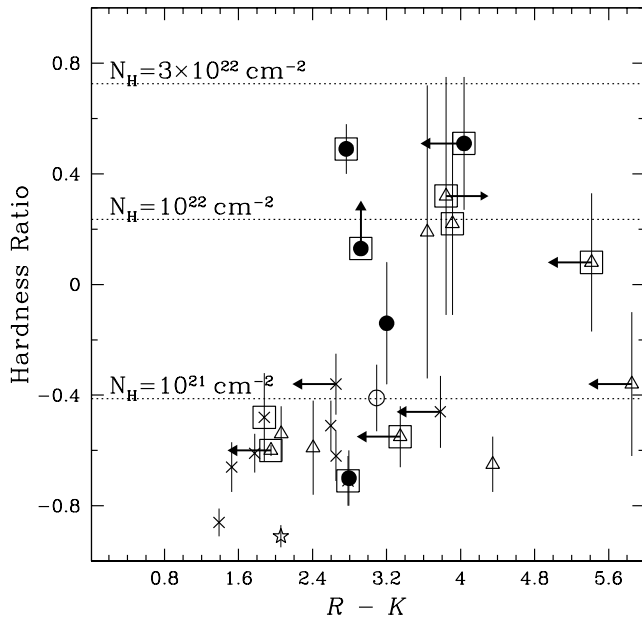


Figure 3. Hardness ratio against $R-K$ colour. The symbols are the same as in Figure 1. The horizontal lines are the expected hardness ratio of a power-law spectral energy distribution with $\Gamma = 1.7$ and different absorbing column densities in the range 0.1 to $3 \times 10^{22} \text{ cm}^{-2}$.

auxiliary files of individual sources were combined using the ADDARF task of FTOOLS. Using the XSPEC v11.2 software, we fit a single power-law to the data absorbed by the Galactic column of $2 \times 10^{20} \text{ cm}^{-2}$ (wabs*pow). The results are presented in Table 3. X-ray/radio matched AGNs have flatter spectra ($\Gamma = 1.78_{-0.03}^{+0.05}$) than non-radio detected sources ($\Gamma = 2.00_{-0.04}^{+0.03}$) at the $\approx 4\sigma$ significance level. A similar result was obtained by Bauer et al. (2002), who explored the association between the faint X-ray (0.5–8 keV) and radio (1.4 GHz) source populations detected in the Hubble Deep Field North region using the 1 Ms *Chandra* dataset and ultra-deep VLA observations. Although their sample is dominated by starbursts, they also identify a number of X-ray selected AGNs and argue that those with radio detections have harder X-ray spectral properties than radio undetected ones. Bauer et al. (2002) suggest that the enhanced absorption observed in radio detected AGNs is due to nuclear starbursts.

We explore this scenario using X-ray spectral fitting analysis of the hard (rest-frame $N_{\text{H}} > 10^{22} \text{ cm}^{-2}$) X-ray/radio matched sources in the Phoenix/XMM-*Newton* survey. Although individual sources have a small number of counts, which do not allow detailed spectral analysis, we can combine their X-ray spectra to study their mean properties. The different redshifts of individual sources may however, dilute the spectral features in the coadded X-ray spectrum. To avoid this effect we only combine the X-ray spectra of sources #7, #22 and #42 in Table 1 that lie at similar redshifts (≈ 0.4). The individual PN X-ray spectra of these 3 sources are shown in Figure A3 of the Appendix.

The 3 spectra are merged using the method described above. We fit a single absorbed power-law (wabs*pow) to

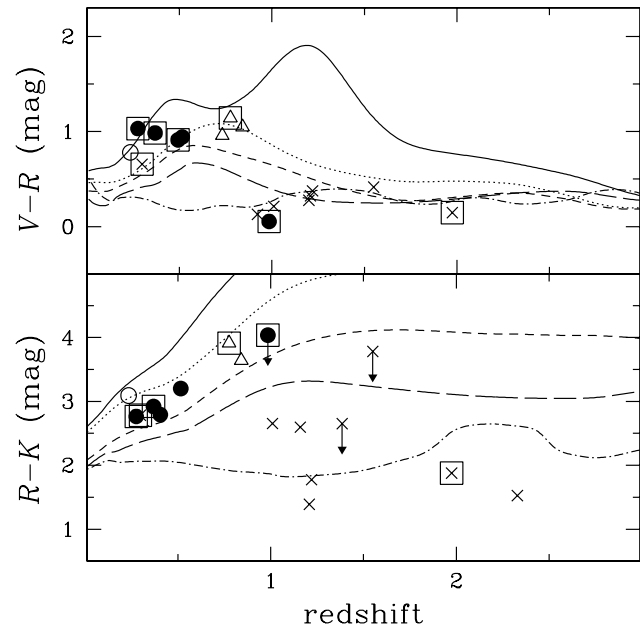


Figure 4. $V-R$ (top panel) and $R-K$ colour (bottom panel) against redshift. The symbols are the same as in Figure 1. The curves are different template SEDs for E/S0 (continuous), Sbc (dotted), Scd (short dashed), irregulars (long dashed) and QSOs (dot-dashed). The galaxy templates are observed SEDs from Coleman, Wu & Weedman (1980). The QSO template is obtained from the set of QSO SEDs of the LE PHARE software. The majority of the sources with the harder X-ray spectra have optical/NIR colours consistent with those of galaxies.

the data with both Γ and N_{H} free parameters. We find $\Gamma \approx 1.9$, $N_{\text{H}} \approx 7 \times 10^{22} \text{ cm}^{-2}$ (not corrected for redshift) and reduced $\chi^2 = 2.02$ for 27 degrees of freedom. The results are shown in Figure 6. This model does not provide a good fit to data and cannot account for the soft excess below about 2 keV in Figure 6. We add a second absorbed power law component (wabs*pow+wabs*pow) with fixed $\Gamma = 1.9$ and absorbing column tied to the Galactic value $N_{\text{H}} \approx 2 \times 10^{20} \text{ cm}^{-2}$. We also fix the power-law index of the first component to $\Gamma = 1.9$, leaving N_{H} a free parameter. This gives $N_{\text{H}} \approx 8.9 \times 10^{22} \text{ cm}^{-2}$ (observer’s frame) and reduced $\chi^2 = 1.28$ for 27 degrees of freedom. We use the F-test to compare the single and two component models above and find that the probability of the two models being an equally good representation of the data is 8.4×10^{-4} . The single component model can therefore be rejected at 99.92 per cent confidence level corresponding to about 2.8σ . If we use an absorbed Raymond-Smith model (wabs*ray+wabs*pow) with a temperature of 0.7 keV (Franceschini et al. 2003) as the second component, we estimate a lower F-test probability (1.6×10^{-2}) corresponding to a rejection significance of $\approx 2.4\sigma$.

The results above are summarised in Table 4 and suggest the presence of a soft component in at least the low- z sub-sample of the X-ray/radio matched AGNs, albeit at the $\approx 2.5\sigma$ level. This component may be associated with scattered emission that is frequently observed in local obscured Seyfert-2 type AGNs (e.g. Turner et al. 1997). In this picture

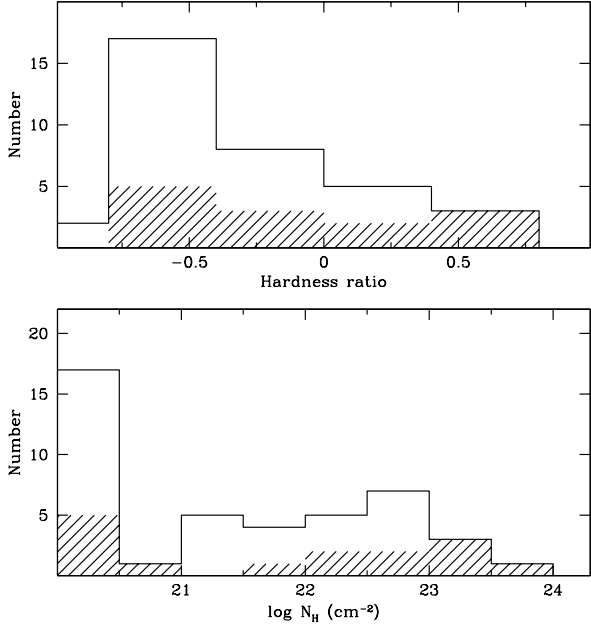


Figure 5. Top: Hardness ratio distribution of the hard X-ray selected sample (open histogram) in comparison with that of X-ray/radio matches (shaded histogram). **Bottom:** rest frame column density distribution of the hard X-ray selected sample (open histogram) in comparison with that of X-ray/radio matches (shaded histogram). Both plots suggest an increasing fraction of radio emitting hard X-ray sources with increasing hardness ratios or absorbing column density.

Figure 6. The merged X-ray spectrum of the 3 heavily obscured (rest frame $N_{\text{H}} > 10^{22} \text{ cm}^{-2}$) radio emitting AGNs at $z \approx 0.4$ (sources #7, 22 and 42 in Table 1). For clarity we only show the PN coadded spectrum. The continuous line is the single absorbed power-law (wabs*pow) model. There is clearly an excess above the single component model at energies $< 2 \text{ keV}$.

AGN sample	number of sources	Γ	χ^2	d.o.f.
X-ray/radio	14	$1.78^{+0.05}_{-0.03}$	1.17	314
X-ray	28	$2.00^{+0.03}_{-0.04}$	1.15	431

Table 3. The mean X-ray spectral properties of the X-ray selected AGNs with and without radio identifications. The X-ray spectra of the two subsamples are fit by an absorbed power-law with the N_{H} fixed to the Galactic value.

there is a thick screen of obscuring material which swamps the soft X-rays while the more energetic hard X-rays can penetrate through. The soft X-ray emission arises from scattering on a pure electron medium.

Alternatively, the soft component may be associated with star-formation activity. We estimate that this component is responsible for about 10 per cent of the 0.5–8 keV luminosity of the stacked spectrum. Since the 3 low- z X-ray/radio matched sources have luminosities of $\approx 10^{43} \text{ erg s}^{-1}$, the above fraction translates to a 0.5–8 keV luminosity of about $10^{42} \text{ erg s}^{-1}$ consistent with that of extreme starbursts in the local Universe (e.g. Moran, Lehnert & Helfand 1999; Georgakakis et al. 2003). We also estimate an upper limit to the star-formation rate of $\text{SFR} = 100 \text{ M}_{\odot} \text{ yr}^{-1}$ for these systems, using the relation between radio luminosity density and SFR (Bell et al. 2003). Any ongoing SFR is most likely lower than the limit above since the AGN will also contribute to the observed radio emission. A SFR of $100 \text{ M}_{\odot} \text{ yr}^{-1}$ is nevertheless, not unreasonably high for a starburst galaxy (e.g. Moran et al. 1999; Ranalli, Comastri & Setti 2003).

4.3 Contribution to the XRB

Summing the X-ray fluxes of individual sources (after correcting for vignetting) from $f_{\text{X}}(2 - 8 \text{ keV}) = 1.24 \times 10^{-13} \text{ erg s}^{-1} \text{ cm}^{-2}$ (i.e. brightest source) to the limit $f_{\text{X}}(2 - 8 \text{ keV}) = 7.7 \times 10^{-15} \text{ erg s}^{-1} \text{ cm}^{-2}$, we estimate a resolved flux of $(6.8 \pm 1.3) \times 10^{-12} \text{ erg s}^{-1} \text{ deg}^{-2}$ assuming Poisson statistics for the errors. This corresponds to $38 \pm 7 - 52 \pm 10$ per cent of the 2–8 keV XRB measured by BeppoSAX (Vecchi et al. 1999) and ASCA (Ueda et al. 1999) respectively. For sources brighter than $f_{\text{X}}(2 - 8 \text{ keV}) = 1.24 \times 10^{-13} \text{ erg s}^{-1} \text{ cm}^{-2}$ (i.e. not probed in our relatively small solid angle survey) we extrapolate the Baldi et al. (2002) best fit relation to estimate a contribution of $\approx 3 \times 10^{-12} \text{ erg s}^{-1} \text{ deg}^{-2}$ or about 16–23 per cent of the total XRB.

For the X-ray sources with radio counterparts we estimate a total flux contribution from the X-ray/radio matched population of $(2.6 \pm 11.0) \times 10^{-12} \text{ erg s}^{-1} \text{ deg}^{-2}$ or $14 \pm 6 - 20 \pm 8$ per cent of the XRB for the BeppoSAX and ASCA normalisations respectively. X-ray/radio matched sources represent about 38 ± 16 per cent of the XRB fraction resolved in our survey for fluxes in the range $f_{\text{X}}(2 - 8 \text{ keV}) = 7.7 \times 10^{-15} - 1.24 \times 10^{-13} \text{ erg s}^{-1} \text{ cm}^{-2}$ of the present survey. Radio emitting AGNs are therefore, a non-negligible fraction of the X-ray background. We also note, that this fraction is skewed by the bright sources in the sample. Ex-

1st component		2nd component	χ^2	d.o.f.
$\Gamma = 1.86^{+0.41}_{-0.44}$	power-law	—	2.02	27
	$N_{\text{H}} = 7.0^{+1.8}_{-1.7} \times 10^{22} \text{ cm}^{-2}$	—		
$\Gamma = 1.9$ (fixed)	power-law	power law	1.28	27
	$N_{\text{H}} = 8.9^{+2.7}_{-2.0} \times 10^{22} \text{ cm}^{-2}$	$N_{\text{H}} = 2 \times 10^{20} \text{ cm}^{-2}$ (fixed)		
$\Gamma = 1.9$ (fixed)	power-law	Raymond-Smith	1.417	26
	$N_{\text{H}} = 7.4^{+2.2}_{-1.5} \times 10^{22} \text{ cm}^{-2}$	kT=0.7 (fixed) $N_{\text{H}} = 2 \times 10^{20} \text{ cm}^{-2}$ (fixed)		

Table 4. The mean X-ray spectral properties of the 3 X-ray sources with radio counterparts that lie at similar redshifts ($z \approx 0.4$). Different model components are used to fit the coadded spectrum.

cluding the two brightest sources (both of which show radio emission) we estimate that the X-ray/radio matched population sums up to about 24 ± 8 per cent of the XRB resolved in the flux range of our survey. Within the 1σ uncertainties however, this is in agreement with the fraction estimated above taking into account the bright sources in the sample.

Barger et al. (2001) combined a Chandra survey of the SSA13 region (limiting flux $f_X(2 - 10 \text{ keV}) = 4 \times 10^{-15} \text{ erg s}^{-1} \text{ cm}^{-2}$) with deep radio observations to a 5σ limiting flux density of $25 \mu\text{Jy}$. They estimate a contribution of the X-ray/radio matched population to the XRB of ≈ 26 per cent. Although this is somewhat higher than the fraction estimated above (14-20 per cent), the difference is likely due to their deeper radio and X-ray data when compared to the Phoenix/XMM-Newton survey.

5 DISCUSSION

Using the Phoenix/XMM-Newton survey, we have presented evidence for a higher fraction of X-ray/radio matches among the obscured AGN population compared to sources with softer X-ray spectral properties. Small number statistics however, limit the significance of this result to the 2σ level.

Previous studies also suggest a higher fraction of obscured AGNs within the X-ray/radio matched population. Ciliegi et al. (2003) find that the fraction of X-ray sources with radio counterparts is higher in hard rather than soft X-ray selected samples. This is attributed to both observational effects (e.g. deeper radio data compared to the X-ray flux limit for the harder samples) and the hard band selection. They argue that both the hard X-ray energies and the radio wavelengths are least biased by dust. Selection at radio and hard X-ray wavelengths therefore provides more complete AGN samples that include obscured AGNs likely to be missed in soft X-ray surveys. Similarly, Barger et al. (2001) found that as much as 50 per cent of their hard X-ray sources to the limit $f_X(2 - 10 \text{ keV}) = 4 \times 10^{-15} \text{ erg s}^{-1} \text{ cm}^{-2}$ have radio counterparts above the 5σ flux density level of $S_{1.4} = 25 \mu\text{Jy}$. Moreover about half of their X-ray/radio matched sources show flat X-ray spectra ($\Gamma \lesssim 1$) suggesting enhanced photoelectric absorption.

A circum-nuclear starburst is an alternative scenario for the higher fraction of X-ray/radio matches within the X-ray harder population. Indeed, since the sub-mJy radio data are sensitive to star-formation activity it may be possible that the hard X-ray/radio matches are composite systems comprising both a central AGN and a nuclear starburst that

both feeds and obscures the central engine (e.g. Fabian et al. 1998).

The coadded X-ray spectra of the 3 low- z hard X-ray selected sources with radio counterparts show evidence for the presence of a soft component, albeit at the $\approx 2.5\sigma$ level. Although this soft excess may be associated with reflection on the dusty torus (Reeves et al. 1997) or scattering on a pure electron medium (Turner et al. 1997) an alternative scenario is star-formation activity. In the local Universe there is a wealth of observational data that suggest a link between circum-nuclear starbursts and AGNs. For example the featureless UV continua of Seyfert 2s have been proposed to be largely produced by a nuclear starburst (Heckman et al. 1995, 1997; Gonzalez-Delgado et al. 1998). More recently, Gonzalez Delgado et al. (2001) and Storchi-Bergmann et al. (2000) estimated that about 30-50 per cent of their Seyferts 2 samples have near-UV spectra that show evidence for the existence of nuclear starbursts. Similarly, the identification of the Ca II triplet in the NIR spectra of Seyfert 2s has been interpreted as evidence for the presence of young stars that are likely to dominate the NIR emission of these systems (e.g. Terlevich, Diaz & Terlevich 1990).

The radio and FIR properties of many Seyfert galaxies are also consistent with starburst activity (Norris, Allen & Roche 1988). Bransford et al. (1998) showed that about 40 per cent of their sample, comprising mostly Seyfert 2s, has radio morphology and/or radio-to-FIR flux ratios suggesting star-formation in addition to the central AGN activity. Ulvestad & Ho (2001) explored the FIR and radio properties of Seyfert 1 and 2s compiled from the Palomar optical spectroscopic survey of nearby galaxies (Ho, Filippenko & Sargent 1995). They find that the radio-to-FIR flux ratio of many Seyfert 2s in their sample, particularly the less luminous ones, is consistent with star-formation. This is somewhat contradictory to the conclusions of Cid Fernandes et al. (2001) and Kauffman et al. (2003) who argue that it is the most powerful (e.g. more far-infrared luminous) Seyfert 2s that show evidence for the presence of young stars.

Moreover, although a number of nearby galaxies (e.g. NGC 6240, NGC 4945) have properties consistent with starburst/LINER activity, observations at hard X-ray wavelengths have revealed a heavily obscured AGN that is hidden from view at any other wavelength (Iwasawa et al. 1993; Iwasawa & Comastri 1998). Such ‘‘composite’’ (starburst+AGN) objects have also been proposed as a significant mode of the XRB (Fabian et al. 1998).

Studies of the X-ray properties of luminous infrared galaxies (LIGs; $L_{\text{FIR}} > 10^{11} L_{\odot}$), believed to be the lo-

cal counterparts of the more distant sub-mJy and μ Jy radio population, also suggest a close link between star-formation and AGN activity. Risaliti et al. (2000) propose a model that invokes a mixture of obscured AGN and starburst activity to reproduce the FIR and X-ray properties of LIGs. Franceschini et al. (2003) used the XMM-*Newton* data to investigate the X-ray spectral properties of a small sample of 10 ultra-luminous infrared galaxies (ULIGs; $L_{FIR} > 10^{12} L_{\odot}$). All the systems in their sample show evidence for thermal hot plasma emission below ≈ 1 keV likely to be associated with a nuclear or a circum-nuclear starburst in agreement with our results. They also find that about half of the sources have X-ray spectral properties suggesting heavily obscured AGN activity.

At higher redshifts Bauer et al. (2002) also suggested the presence of nuclear star-formation activity in X-ray selected AGNs with radio counterparts on the basis of both their X-ray and radio properties. Additionally they show that X-ray/radio matched AGNs have flatter X-ray spectra than AGNs without radio emission in agreement with our results. Radio loud AGNs have also been found to have flatter X-ray spectral properties ($\Gamma = 1.6$) than radio quiet ones (Reeves & Turner 2000; Gambill et al. 2003). We note, however, that most of the X-ray/radio matched sources in the present study are either radio-quiet or lie on the borderline between radio-loud and radio-quiet systems. Furthermore, the majority of the sources in the studies above are more luminous at both X-ray, optical and radio wavelengths than the systems presented here. Most show broad optical emission lines, while our X-ray/radio matched population with hard X-ray spectral properties and available optical spectroscopy have narrow optical emission lines. This suggests that the absorbed population studied here is different from the radio loud QSO samples of Reeves & Turner (2000) and Gambill et al. (2003).

6 CONCLUSIONS

In this paper we have explored the radio properties of hard X-ray selected sources using a deep (50 ks) XMM-*Newton* pointing overlapping with a subregion of a deep and homogeneous radio survey (the Phoenix Deep Survey) reaching μ Jy sensitivities. A total of 43 sources are detected above the X-ray flux limit $f_X(2 - 8 \text{ keV}) = 7.7 \times 10^{-15} \text{ erg s}^{-1} \text{ cm}^{-2}$, with 14 associated with radio sources. A total of 29 hard X-ray selected sources are optically identified using either relatively shallow ($R = 22.5$ mag) or deeper ($R \approx 24$ mag) optical data. Spectroscopic data are available for 18 of the optically brighter X-ray sources.

The hard X-ray selected sample comprises (i) 11 AGNs with broad emission lines, 2 of which are associated with a radio source (ii) 6 systems with narrow emission line optical spectra, 4 of which also have radio emission, (iii) 1 galaxy with absorption optical lines, (iv) 1 Galactic star candidate on the basis of its optical and X-ray properties, (v) 12 sources with optical identification but no spectroscopic redshift measurement and (vi) 12 optically unidentified sources, 2 of which are associated with a radio source. One of the narrow emission line X-ray/radio sources may be a candidate type-2 QSO at $z \approx 0.985$.

We find evidence for an increasing fraction of X-

ray/radio matches with increasing hardness ratio or rest-frame column density, suggesting that radio detected AGNs have, on average, harder X-ray spectral properties. Indeed, X-ray selected AGNs associated with radio counterparts have flatter X-ray spectra than the non radio detected X-ray sources. We argue that the enhanced photoelectric absorption observed in radio emitting X-ray selected AGNs is likely to be associated with circum-nuclear starburst activity that both feeds and obscures the central engine. At least for a small sub-sample of low- z radio emitting AGNs their combined spectrum exhibits a soft X-ray component, albeit at the 2.5σ confidence level, that may be associated with star-formation activity. However, we cannot exclude the reflection on the dusty torus or the scattering on a pure electron medium as alternative scenarios for the observed soft emission. The unparalleled sensitivity of the *Spitzer* observatory can potentially provide more information on the presence of a circum-nuclear starburst in these radio emitting AGNs. Mid-infrared spectroscopy can provide useful diagnostics on the nature of the central source (e.g. Genzel & Cesarsky 2000) while, mid- to far-infrared photometry can constrain the SEDs of these systems allowing one to assess the relative contribution of the starburst and the AGN components (e.g. Farrah et al. 2003). Deeper X-ray observations are also essential to improve the photon statistics and to perform detailed X-ray spectral analysis of these sources.

The optical and NIR colours of the harder X-ray sources are consistent with those of galaxies, suggesting that the optical and the NIR light of this population is dominated by the host galaxy rather than the obscured AGN. By contrast, X-ray sources with soft X-ray spectral properties (many of which are identified with broad optical emission lines) have blue colours consistent with those of Seyfert 1s and QSOs.

Finally, to the limit of the present radio and X-ray data, we find radio emitting AGNs make up a non-negligible fraction of the XRB. About $14 \pm 6 - 20 \pm 8$ per cent of the total XRB for the BeppoSAX and ASCA normalisations respectively arises in AGNs associated with radio emission. About half of this fraction arises from sources with hard X-ray spectral properties, suggesting enhanced absorption.

7 ACKNOWLEDGMENTS

The authors wish to thank the anonymous referee for constructive comments, Ioannis Georgantopoulos for numerous discussions and for his useful suggestions and Athanassios Akylas for his help with the X-ray spectral fittings. The Phoenix Deep Survey radio data as well as part of the observations presented here are electronically available at <http://www.atnf.csiro.au/people/ahopkins/phoenix/>. AG acknowledges funding by the European Union and the Greek Ministry of Development in the framework of the Programme 'Competitiveness – Promotion of Excellence in Technological Development and Research– Action 3.3.1', Project 'X-ray Astrophysics with ESA's mission XMM', MIS-64564. AMH acknowledges support provided by the National Aeronautics and Space Administration through Hubble Fellowship grant HST-HF-01140.01-A awarded by the Space Telescope Science Institute. JA gratefully acknowledges the support from the Science and Technology Foundation (FCT, Portugal) through the fellowship BPD-5535-

2001 and the research grant POCTI-FNU-43805-2001. MS acknowledges support from a PPARC fellowship.

REFERENCES

Akiyama et al., 2000, ApJ, 532, 700
 Alexander D. M., Brandt W. N., Hornschemeier A. E., Garmire G. P., Schneider D. P., Bauer F. E., Griffiths R. E., 2001, AJ, 122, 2156
 Baldi A., Molendi S., Comastri A., Fiore F., Matt G., Vignali C., 2002, ApJ, 564, 190
 Babbedge T. S. R., et al., MNRAS, accepted, astro-ph/0406296
 Barger A. J., Cowie L. L., Mushotzky R. F., Richards E. A., 2001, AJ, 121, 662
 Barger A. J., Cowie L. L., Brandt W. N., Capak P., Garmire G. P., Hornschemeier A. E., Steffen A. T., Wehner E. H., 2002, AJ, 124, 1839
 Barger, A. J. et al. 2003, AJ, 126, 632
 Bauer F. E., Alexander D. M., Brandt W. N., Hornschemeier A. E., Vignali C., Garmire G. P., Schneider D. P., 2002, AJ, 124, 2351
 Bell E. F., 2003, ApJ, 586, 794
 Bertin E. & Arnouts S., 1996, A&AS, 117, 393
 Bolzonella M., Miralles J.-M., Pelló R., 2000, A&A 363, 476
 Brandt W. N., et al., 2001, AJ, 122, 2810
 Bransford M. A., Appleton P. N., Heisler C. A., Norris R. P., Marston A. P., 1998, ApJ, 497, 133
 Brinkmann W., Laurent-Muehleisen S. A., Voges W., Siebert J., Becker R. H., Brotherton M. S., White R. L., Gregg M. D., 2000, A&A, 356, 445
 Cash W., 1979, ApJ, 228, 939
 Cid Fernandes R. Jr., Heckman T. M., Schmitt H. R., González Delgado R. M., Storchi-Bergmann T., 2001, ApJ, 558, 81
 Ciliegi P., Vignali C., Comastri A., Fiore F., La Franca F., Perola G. C., 2003, MNRAS, 342, 575
 Coleman G. D., Wu C.-C., Weedman D. W., 1980, ApJ, 43, 393
 Cristiani S., Vio R., 1990, A&A, 227, 385
 Cristiani S., et al., 2004, ApJ, 600, L119
 Dickey J. M. & Lockman F. J., 1990, ARA&A, 28, 215
 Downes A. J. B., Peacock J. A., Savage A., Carrie D. R., 1986, MNRAS, 218, 31
 Fabian A. C., Barcons X., Almaini O., Iwasawa K., 1998, MNRAS, 297L, 11
 Farrah D., Afonso J., Efstathiou A., Rowan-Robinson M., Fox M., Clements D., 2003, MNRAS, 343, 585
 Fiore F., 2003, A&A, 409, 79
 Franceschini A. et al., 2003, MNRAS, 343, 1181
 Gambill J. K., Sambruna R. M., Chartas G., Cheung C. C., Maraschi L., Tavecchio F., Urry C. M., Pesce J. E., 2003, A&A, 401, 505
 Gandhi P., Crawford C. S., Fabian A. C., Johnstone R. M., 2004, MNRAS, in press; astro-ph/0310772
 Gardner J. P., Cowie L. L., Wainscoat R. J., 1993, ApJ, 415L, 9
 Genzel R., Cesarsky C. J., 2000, ARA&A, 38, 761
 Georgantopoulos I., Georgakakis A., Akylas A., Stewart G. C., Giannakis O., Shanks T., Kitsionas S., 2004, MNRAS, submitted, astro-ph/0406346
 Georgakakis A., Mobasher B., Cram L., Hopkins A., Lidman C., Rowan-Robinson M., 1999, MNRAS, 306, 708
 Georgakakis A., Hopkins A. M., Sullivan M., Afonso J., Georgantopoulos I., Mobasher B., Cram L. E., 2003, MNRAS, 345, 939
 Giacconi R., et al., 2002, ApJS, 139, 369
 Glazebrook K., Peacock J. A., Collins C. A., Miller L., 1994, MNRAS, 266, 65

González Delgado R. M., Heckman T., Leitherer C., Meurer G., Krolik J., Wilson A. S., Kinney A., Koratkar A., 1998, ApJ, 505, 174
 Heckman T., et al., 1995, ApJ, 452, 549
 Heckman T. M., Gonzalez-Delgado R., Leitherer C., Meurer G. R., Krolik J., Wilson A. S., Koratkar A., Kinney A., 1997, ApJ, 482, 114
 Ho L. C., Filippenko A. V. & Sargent W. L. W., 1995, ApJS, 98, 477
 Hopkins A. M., Miller C. J., Connolly A. J., Genovese C., Nichol R. C., Wasserman L., 2002, AJ, 123, 1086
 Hopkins A. M., Afonso J., Chan B., Cram L. E., Georgakakis A., Mobasher B., 2003, AJ, 125, 465
 Hopkins A., Afonso J., Cram L., Mobasher B., 1999, ApJ, 519L, 59
 Hopkins A. M., Mobasher B., Cram L., Rowan-Robinson M., 1998, MNRAS, 296, 839H
 Isobe T., Feigelson E. D., Nelson P. I., 1986, ApJ, 306, 490
 Iwasawa K., Koyama K., Awaki H., Kunieda H., Makishima K., Tsuru T., Ohashi T., Nakai N., 1993, ApJ, 409, 155
 Iwasawa K. & Comastri A., 1998, MNRAS, 297, 1219
 Kauffmann G., et al., 2003, MNRAS, 346, 1055
 Kitsionas S., Hatziminaoglou E., Georgakakis A., Georgantopoulos I., 2004, MNRAS, submitted
 Laor A., Fiore F., Elvis M., Wilkes B. J., McDowell J. C., 1997, ApJ, 477, L93
 LaValley M., Isobe T., Feigelson E. D., 1992, BAAS, 24, 839
 Mainieri V. et al., 2002, A&A, 393, 425
 McHardy I. et al., 2003, MNRAS, 342, 802
 Mobasher B., et al., 2004, ApJ, 600L, 167
 Moran E. C., Lehnert M. D., Helfand D. J., 1999, ApJ, 526, 649
 Morrison R., McCammon D., 1983, ApJ, 270, 119
 Norris R. P., Allen D. A., Roche P. F., 1998, MNRAS, 234, 773
 Persson S. E., Murphy D. C., Krzeminski W., Roth M., Rieke M. J., 1998, AJ, 116, 2475
 Piconcelli E., Cappi M., Bassani L., Di Cocco G., Dadina M., 2003, A&A, 412, 689
 Ranalli P., Comastri A., Setti G., 2003, A&A, 399, 39
 Raymond J. C., Smith B. W., 1977, ApJS, 35, 419
 Reeves J. N., Turner M. J. L., 2000, MNRAS, 316, 234
 Reeves J. N., Turner M. J. L., Ohashi T., Kii T., 1997, MNRAS, 292, 468
 Richards G. T., et al., 2001, AJ, 122, 1151
 Risaliti G., Gilli R., Maiolino R., Salvati M., 2000, A&A, 357, 13
 Risaliti G., Marconi A., Maiolino R., Salvati M., Severgnini P., 2001, A&A, 371, 37
 Risaliti G., Elvis M., Gilli R., Salvati M., 2003, ApJ, 587, 9L
 Stocke J. T., Morris S. L., Weymann R. J., Foltz C. B., 1992, ApJ, 396, 487
 Storchi-Bergmann T., Raimann D., Bica E. L. D., Fraquelli H. A., 2000, ApJ, 544, 747
 Strüder L., Briel U., Dennerl K., et al. 2001, A&A, 365, L18
 Sullivan M., Hopkins A. M., Afonso J., Georgakakis A., Mobasher B., Cram L. E., 2004, ApJS, in press
 Terlevich E., Diaz A. I., Terlevich R., 1990, MNRAS, 242, 271
 Turner T. J., George I. M., Nandra K., Mushotzky R. F., 1997, ApJS, 113, 23
 Turner M. J. L., Abbey A., Arnaud M., et al., 2001, A&A, 365, L27.
 Ueda Y., 1999, ApJ, 518, 656
 Ulvestad J. S., Ho L. C., 2001, ApJ, 558, ????
 Vecchi A., Molendi S., Guainazzi M., Fiore F., Parmar A. N., 1999, A&A, 349L, 73

APPENDIX A: NOTES ON SELECTED SOURCES

In this section we discuss in more detail the properties of the X-ray sources with radio identification and available spectroscopic information. In addition to these sources we also discuss the properties of the candidate star (source #25) identified in our sample.

#7: This source has a narrow emission line optical spectrum at $z = 0.276$ (see Figure A1). The relative strengths of the H β and [O III] 5007Å emission lines as well as the presence of high excitation lines (e.g [Ne III] 3869, [Ne V] 3426 Å) suggest obscured AGN activity. This is consistent with the flat X-ray spectrum suggesting a rest frame absorbing column of $\approx 4 \times 10^{22} \text{ cm}^{-2}$ ($\Gamma = 1.7$). The optical *R*-band image with the X-ray and the radio positions overlaid are shown in Figure A2. Visual inspection of the *R*-band image shows two components likely to be in the process of interaction/merging.

#12: This source is assigned a redshift $z = 0.985$ on the basis of a single narrow emission line interpreted as [O II] 3727 Å. The X-ray spectrum suggests a high column density $N_{\text{H}} = 1.3 \times 10^{23} \text{ cm}^{-2}$ ($\Gamma = 1.7$). The X-ray luminosity of this source at $z = 0.985$ before applying any correction due to intrinsic photoelectric absorption is estimated $L_X(2 - 8 \text{ keV}) \approx 10^{44} \text{ erg s}^{-1}$. The evidence above suggests a candidate type-2 QSO. Interestingly, the optical colour of this source is very blue $V - R \approx 0 \text{ mag}$. This is hard to reconcile with the heavily absorbed X-ray spectrum suggesting significant amounts of dust. It is possible that the very blue optical colour is associated with starburst activity in the host galaxy. The optical spectrum and the optical *R*-band image with the X-ray and the radio positions overlaid are shown in Figures A1 and A2 respectively.

#13, 23: These 2 sources have broad emission line systems with soft X-ray spectral properties. They are associated with radio sources, albeit below the formal $80 \mu\text{Jy}$ radio detection level corresponding to about 5σ . The optical spectra and the optical images of these sources are shown in Figures A1 and A2 respectively.

#22: This source has properties very similar to those of #7. At $z = 0.369$ it also has a narrow emission line optical spectrum (see Figure A1) with relative line strengths suggesting obscured AGN activity. This is also consistent with the hard X-ray spectral properties of this source suggesting a rest-frame column density $N_{\text{H}} = 1.6 \times 10^{23} \text{ cm}^{-2}$. The optical *R*-band image of this source with X-ray and the radio positions overlaid are also shown in Figure A2.

#25: This X-ray source is associated with an unresolved bright $R \approx 13 \text{ mag}$ optical source, most likely a Galactic star. The observed X-ray-to-optical flux ratio is estimated ≈ -3 , while the X-ray spectrum of this source is best fit by a Raymond-Smith model with $kT = 0.70_{-0.05}^{+0.06}$ and abundance $0.038_{-0.010}^{+0.017}$ ($\chi^2 = 1.5$ for 81 degrees of freedom). This source is not shown in Figure A2 although its X-ray spectrum is plotted in A3

#32: This X-ray source is associated with a pair of optical galaxies likely to be interacting (see Figure A2). This source has been observed by HYDRA yielding the featureless spectrum shown in Figure A1 that did not allow a redshift determination. The evidence above in combination with the soft X-ray spectral properties of source #32 may sug-

gest a BL-Lac. However, the two point radio/optical and X-ray/optical indices of this source ($\alpha_{OX} = 1.02$, $\alpha_{RO} = 0.09$) are not consistent with those expected for BL-Lacs (Stoche et al. 1991).

#42: This source has a narrow emission line spectrum presented in Figure A1. The relative strengths of the H β and [O III] 5007Å emission lines suggest obscured AGN activity. This is also confirmed by the hard X-ray spectral properties of this source suggesting an rest-frame column density of $N_{\text{H}} \approx 2 \times 10^{23} \text{ cm}^{-2}$ ($\Gamma = 1.7$). The optical *R*-band image of this source with X-ray and the radio positions overlaid are shown in Figure A2.

Figure A1. Optical spectra of the X-ray/radio matches. The intensity shown is the observed count rate, since we have not performed flux calibration (see section 2.4).

Figure A2. Optical *R*-band images of the X-ray/radio matches. The circle has a radius of 5 arcsec and is centered at the position of the X-ray source centroid. The square has a side of 7 arcsec and shows the radio source position.

Figure A3. X-ray spectra of individual X-ray/radio matches with optical spectroscopy. For clarity we show only the PN spectrum. The curves are the wabs**pow* models described in section 3 with the parameters listed in Table 2. In the case of C-statistic (sources #7, 12, 22, 42) we fix the exponent Γ to 1.7 and fit the N_H . In the case of χ^2 analysis (sources #13, 23, 25, 32) both the Γ and the N_H of the wabs**pow* model are free parameters. The only exception is the candidate Galactic star, source #25, for which we show the best fit Raymond-Smith model. The reduced χ^2 for sources #13, 23, 25, 32 is respectively 1.55, 0.76, 1.5 and 1.14 for 28, 27, 81 and 224 degrees of freedom respectively.

This figure "figureA1.jpeg" is available in "jpeg" format from:

<http://arxiv.org/ps/astro-ph/0407078v1>

This figure "figureA2.jpeg" is available in "jpeg" format from:

<http://arxiv.org/ps/astro-ph/0407078v1>

This figure "figureA3.jpeg" is available in "jpeg" format from:

<http://arxiv.org/ps/astro-ph/0407078v1>

This figure "figure6.jpeg" is available in "jpeg" format from:

<http://arxiv.org/ps/astro-ph/0407078v1>